A theoretical approach to
the passive control of spiral vortex breakdown

Ubaid A. Qadri and Matthew P. Juniper
Department of Engineering
University of Cambridge
Cambridge, UK CB2 1PZ
Email:uaq20@cam.ac.uk

Abstract—Previous numerical simulations have shown that vortex breakdown starts with the formation of a steady axisymmetric bubble and that an unsteady spiralling mode then develops on top of this. We study how this spiral mode of vortex breakdown might be suppressed or promoted. We use a Lagrangian approach to identify regions of the flow which are sensitive to small open-loop steady and unsteady (harmonic) forces. We find these regions to be upstream of the vortex breakdown bubble. We investigate passive control using a small axisymmetric control ring. In this case, the steady and unsteady control forces are caused by the drag force on the control ring. We find a narrow region upstream of the bubble where the control ring will stabilise the flow and we verify this using numerical simulations.

Index Terms—flow control, vortex breakdown, passive control, adjoint, sensitivity analysis

I. INTRODUCTION

Vortex breakdown has been observed in many practical flows, such as the flow over the leading edge of delta wings at high angles of attack, the injection of fuel and air into combustion chambers, and the intense rotating flow found in a tornado. In all these cases, when the fluid rotates with sufficient azimuthal velocity (swirl), a stagnation point and a recirculation bubble form within it. The transition from the flow without a breakdown bubble to the flow with a breakdown bubble is labelled *axisymmetric* vortex breakdown. In many cases, a spiral structure is seen to emanate and grow downstream of the breakdown bubble. This is labelled *spiral* vortex breakdown.

Vortex breakdown was first observed in the flow over gothic and delta wings at high angles of attack in 1957 [1]. Since then, several different forms of vortex breakdown have been observed in a variety of experimental settings such as tubes, nozzles, and combustion chambers. Investigators often observed the axisymmetric and spiral modes of breakdown to occur almost simultaneously. This led to disagreements over the nature of vortex breakdown. Recent numerical studies of vortex breakdown in an unconfined domain [2], [3], however, have confirmed that the basic form of vortex breakdown is axisymmetric and that the spiral mode is caused by the self-sustained growth of helical perturbations on top of the breakdown bubble. This is a global instability.

The importance of the vortex breakdown phenomenon means that there is a need to understand and control it. In the past, various open-loop control strategies have been attempted [4]. These include active flow control using blowing and suction, and passive flow control using mechanical devices in the flow. However, their success has always been limited due to insufficient knowledge of the physical mechanisms that are at work. To this end, numerical sensitivity analyses have been successful in predicting how one might control vortex shedding off cylinders and other blunt bodies at moderate Reynolds numbers [5]–[8]. These sensitivity analyses use adjoints to calculate the receptivity of the flow to external forcing and the sensitivity of the flow to internal feedback. They can provide information about the effect of steady and harmonic forces on the unstable mode. Hence they have been used to predict where a control device should be placed to either suppress or promote vortex shedding.

In this paper, we carry out a similar analysis around the axisymmetric vortex breakdown state and predict how the spiral mode of vortex breakdown might be suppressed or promoted. In Section II, we consider the stability of the axisymmetric breakdown state and show that spiral vortex breakdown is caused by a linear global instability. In Section III, we use adjoints to evaluate the effect of a small control force on the growth rate of the unstable mode and identify the regions of the flow that are most sensitive to a control force. In Section IV, we apply these results to the simple case of passive control using a small axisymmetric control ring. Finally, in Section V, we discuss how these techniques can be applied in practice.

This study is at $Re = 200$ and the primary motivation is scientific. There are important industrial motivations, however. Vortex breakdown occurs in wingtip vortices behind aircraft, in vacuum cleaners, and in gas turbine combustion chambers. In the case of combustion chambers, hydrodynamic instabilities in the flow can lock into acoustic resonances within the combustion chamber, causing high amplitude thermoacoustic instabilities, which can be catastropic. This fundamental study of spiral vortex breakdown will reveal the regions of the flow where control would be most effective. This could help designers devise effective control strategies.
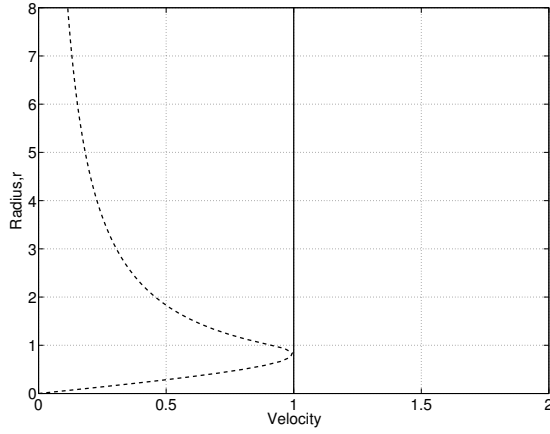
Fig. 1. Non-dimensional inlet velocity distributions for the Grabowski profile: the solid line represents the axial velocity, the dashed line represents the azimuthal velocity for a swirl value of $Sw = 0.915$.
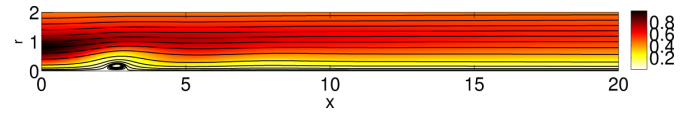

Fig. 2. Steady baseflow at $Sw = 0.915$ and $Re = 200$. The domain extends radially from $-8 \leq r \leq 8$ but only a portion is shown here. There is a small axisymmetric breakdown bubble around $x = 2.5$.
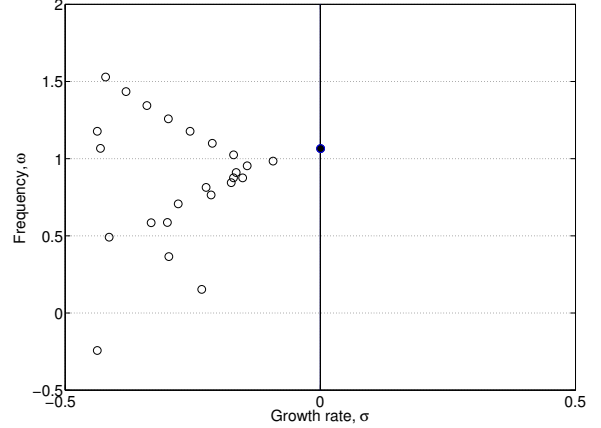

Fig. 3. Spectrum of the linear operator $\mathbf{L}$ for $m = -1$ for the baseflow in Figure 2, showing the 25 least stable eigenvalues. One mode, coloured black, is just unstable.

II. The flow configuration and the global stability analysis

We study the motion of a viscous fluid in a cylindrical domain with length X_{max} and radius R_{max}, using cylindrical coordinates (x, r, θ). The flow has density ρ, pressure p, temperature T, and velocity $\mathbf{u} = (u_x, u_r, u_\theta)^T$. We describe the motion of the flow using the Navier–Stokes equations in the low Mach number limit. This allows for density variations in the flow but excludes acoustic waves. These equations can be expressed in terms of the momentum $\mathbf{m} = \rho\mathbf{u}$, temperature and pressure as

$$\frac{\partial \mathbf{q}}{\partial t} = \mathcal{N}\mathbf{q}, \tag{1}$$

where $\mathbf{q} \equiv (m_x, m_r, m_\theta, T, p)^T$ is the state vector and $\mathcal{N}$ is a nonlinear differential operator representing the action of the equations on the state vector. The density, ρ, is not included in the state vector because it can be derived from the temperature, T.

Along $x = X_{max}$ and $r = R_{max}$, we choose boundary conditions so that we model flow into a semi-infinite domain in the downstream and radial directions. At the inlet to the domain, we impose velocity profiles that have been used to study vortex breakdown numerically in the past [9]. This Grabowski profile, shown in Figure 1, has uniform density and temperature. The ratio of the azimuthal to axial velocities at $r = 1$ defines the swirl parameter, Sw. The Reynolds number is defined in terms of the nominal vortex core radius and uniform axial velocity. In this study, we keep $Re = 200$.

We obtain a steady axisymmetric laminar baseflow, $\bar{\mathbf{q}}$, or equilibrium point of the equations (1) such that

$$\mathcal{N}\bar{\mathbf{q}} = 0, \tag{2}$$

Figure 2 shows the steady baseflow at $Sw = 0.915$. There is a breakdown bubble around $x = 2.5$. The evolution of small perturbations $\mathbf{q}'$ around this field is governed by

$$\frac{\partial \mathbf{q}'}{\partial t} = \mathbf{L}\mathbf{q}', \tag{3}$$

where $\mathbf{L}$ represents the Navier–Stokes equations linearized about the base-flow $\bar{\mathbf{q}}$. We decompose the perturbations into Fourier modes in time and the azimuthal direction

$$\mathbf{q}'(x, r, \theta, t) = \hat{\mathbf{q}}(x, r)e^{\mathrm{i}m\theta + \lambda t}, \tag{4}$$

where m (without a subscript) is the azimuthal wavenumber, and $\lambda \equiv \sigma + \mathrm{i}\omega$ contains the growth rate, σ, and frequency, ω. We study the linear dynamics of the flow by analyzing the eigenvalues of $\mathbf{L}$. These are given by solving the matrix eigenvalue problem

$$\lambda\hat{\mathbf{q}} = \mathbf{L}_m\hat{\mathbf{q}}, \tag{5}$$

where $\mathbf{L}_m$ is the linear operator for the azimuthal wavenumber m. Each of these eigenvalues has a corresponding two-dimensional eigenfunction, $\hat{\mathbf{q}}(x, r)$. We label each eigenvalue/eigenfunction pair a *direct global mode*. If $\sigma > 0$, the mode is linearly globally unstable. In this linear analysis, the flow tends to the form of the global mode with highest σ in the long-time limit and therefore this mode determines the system's overall stability.

Figure 3 shows the eigenvalue spectrum for $m = -1$ at $Sw = 0.915$, for which there is one unstable global mode. All
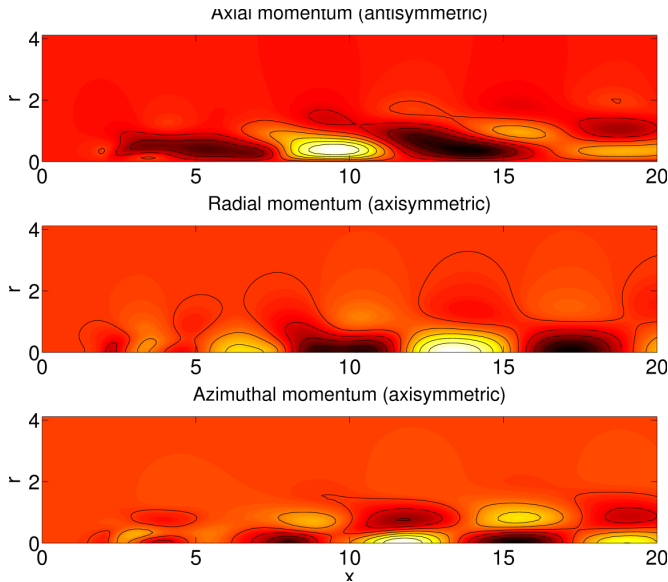
Fig. 4. Spatial structure of the most unstable eigenmode for $m = -1$, showing the real part of the axial, radial and azimuthal momentum in the top half of the domain.

other azimuthal wavenumbers are stable. The spatial structure of the unstable global mode is shown in Figure 4 using the real part of the axial, radial and azimuthal momentum. The imaginary part of the global mode is $1/4$ wavelength out of phase because this mode grows and advects downstream.

III. SENSITIVITY TO A CONTROL FORCE

We now consider open-loop control of the unstable eigenvalue. Depending on the application, engineers might want either to suppress the unstable mode (to delay transition, for instance) or to promote it (to increase mixing, for instance).

To begin with, we evaluate the effect of a small control force on the unstable eigenvalue. We model the control force by adding mass, momentum and energy source terms to the right-hand side of equation (1):

$$\frac{\partial \mathbf{q}}{\partial t} = \mathcal{N}\mathbf{q} + \mathbf{F}. \tag{6}$$

Here, the forcing terms have been grouped together as $\mathbf{F}$. The control force has a steady component ($\bar{\mathbf{F}}$) that acts on the base flow ($\bar{\mathbf{q}}$) and a linearized perturbation ($\mathbf{f}'$) that acts on the linear operator ($\mathbf{L}$) . We model the effects of these two components separately [10].

A. The sensitivity to steady forcing

The eigenvalue of the global mode, $\lambda = \sigma + \mathrm{i}\omega$, is a function of the base flow fields ($\bar{\mathbf{q}}$) and these are, in turn, functions of the steady components of the forcing terms ($\bar{\mathbf{F}}$). The eigenvalue can, thus, be considered to be a function of the steady component of the forcing terms, $\lambda = f(\bar{\mathbf{F}})$. We wish to find the gradient of the functional $\lambda(\bar{\mathbf{F}})$ [8, Fig.9] for

the unstable flow in §II. We investigate the variation of the eigenvalue, $\delta\lambda_{\bar{\mathbf{F}}}$, with respect to small variations of the steady forces, $\delta\bar{\mathbf{F}}$. The change in the eigenvalue is given by

$$\delta\lambda_{\bar{\mathbf{F}}} = \langle \nabla_{\bar{\mathbf{F}}}\lambda, \delta\bar{\mathbf{F}} \rangle, \tag{7}$$

where $\nabla_{\bar{\mathbf{F}}}\lambda$ is a complex function that we call the *sensitivity of the eigenvalue to steady forcing*. The notation $\langle \mathbf{a}, \mathbf{b} \rangle$ denotes an inner product over a volume V,

$$\langle \mathbf{a}, \mathbf{b} \rangle = \frac{1}{V} \int_V \mathbf{a}^H \mathbf{b} \, dV, \tag{8}$$

where $\mathbf{a}^H$ denotes the Hermitian (*i.e.* complex conjugate transpose) of $\mathbf{a}$.

We calculate the sensitivity function by formulating a Lagrangian problem for λ. The nonlinear and linearised Navier–Stokes equations act as constraints in this problem,

$$\mathcal{L} = \lambda - \langle \bar{\mathbf{q}}^+, \mathcal{N}\bar{\mathbf{q}} - \bar{\mathbf{F}} \rangle - \langle \hat{\mathbf{q}}^+, \lambda\hat{\mathbf{q}} - \mathbf{L}_m\hat{\mathbf{q}} \rangle \tag{9}$$

The Lagrange multipliers, $\bar{\mathbf{q}}^+$ and $\hat{\mathbf{q}}^+$, are the adjoint base flow and adjoint global mode fields respectively. We are interested in the functional derivative of $\mathcal{L}$ with respect to $\bar{\mathbf{F}}$. To find this, we first set the functional derivatives of $\mathcal{L}$ with respect to all other variables to zero. This leads to a set of equations that defines an eigenvalue problem for the adjoint global mode, a set of equations for the adjoint base flow fields and the normalization condition $\langle \hat{\mathbf{m}}^+, \hat{\mathbf{m}} \rangle + \langle \hat{T}^+, \hat{T} \rangle = 1$. The analysis then shows that the sensitivity of the eigenvalue to the steady forcing terms is given by the relevant adjoint baseflow field. For example, the sensitivity to momentum forcing is given by the adjoint baseflow momentum, $\bar{\mathbf{m}}^+$.

The adjoint base flow fields are complex valued. The real part represents the sensitivity of the growth rate, σ while the imaginary part represents the sensitivity of the frequency ω to small changes in the steady forcing. They provide information about the most sensitive regions for control based on the physical mechanisms that cause the instability.

The adjoint base flow equations contain terms from the steady base flow, the direct global mode and the adjoint global mode. These need to be calculated before the adjoint base flow equations can be solved. The procedure for obtaining the sensitivity to steady forcing involves the following steps:
1. Obtain a steady base flow (Equation 2 and Figure 2).
2. Obtain the direct global mode by solving the direct eigenvalue problem (Equation 5 and Figure 4).
3. Obtain the adjoint global mode by solving the adjoint eigenvalue problem.
4. Normalize the adjoint global mode.
5. Solve the adjoint base flow equations to obtain the sensitivity of that global mode to steady forcing.

(a) Sensitivity to steady momentum forcing

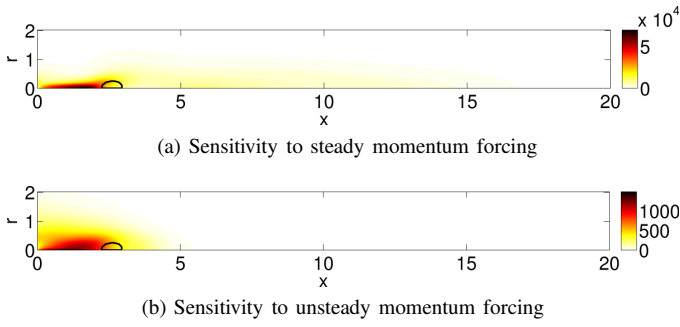(b) Sensitivity to unsteady momentum forcing

Fig. 5. Sensitivity to steady and unsteady forcing for the marginally unstable mode. Darker regions are more sensitive. The thick black line indicates the vortex breakdown bubble. The quantities plotted are (a) The adjoint baseflow momentum $||\bar{\mathbf{m}}^+||$ and (b) the adjoint global mode momentum $||\hat{\mathbf{m}}^+||$

B. Sensitivity to unsteady forcing

The change in the eigenvalue due to a small linearized force ($\delta\mathbf{f}'$) that acts on the linear operator $\mathbf{L}$ is given by

$$\delta\lambda_{\mathbf{f}'} = \langle \nabla_{\mathbf{f}'}\lambda, \delta\mathbf{f}' \rangle, \tag{10}$$

where $\nabla_{\mathbf{f}'}\lambda$ is labelled the *sensitivity of the eigenvalue to harmonic forcing*.

As for the steady forcing terms, the sensitivity of the eigenvalue to harmonic forcing is given by the relevant adjoint global mode fields. The change in the eigenvalue is, thus, simply obtained by projecting the linearized force onto the adjoint global mode fields. The largest change is obtained when the forcing frequency is equal to the frequency of the linear global mode [8, §4.1].

C. Results of sensitivity analysis

Figures 5a and 5b show the sensitivity of the marginally unstable eigenvalue to steady and harmonic forcing respectively. We notice that, for both types of forcing, the flow is most sensitive just upstream of the breakdown bubble. This shows where a control force will have the greatest effect. The scales in the plot indicate that the sensitivity to steady forcing is almost an order of magnitude greater than the sensitivity to harmonic forcing.

IV. PASSIVE CONTROL USING A SMALL CONTROL RING

In this section, we extend the results from the previous section to the specific case of a thin axisymmetric control ring that is placed in the flow. The force on the flow is equal and opposite to the drag force that the control ring experiences. In a cylindrical co-ordinate system, this force can be modelled by the force on a small circular cylinder. As a simple model, the steady and unsteady components of the force due to a cylinder

(a) Magnitude of steady component of control force $||\bar{\mathbf{F}}||/\alpha$

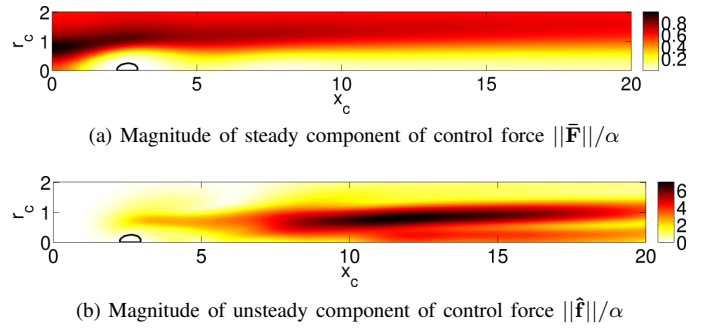(b) Magnitude of unsteady component of control force $||\hat{\mathbf{f}}||/\alpha$

Fig. 6. Magnitude of the steady and unsteady force from a control ring placed in the flow. Darker regions have higher magnitude. The thick black line indicates the vortex breakdown bubble.

placed at (x_c, r_c) are given by

$$\bar{\mathbf{F}}(x,r) = -\alpha||\bar{\mathbf{u}}||\bar{\mathbf{u}}\,\delta(x - x_c, r - r_c), \tag{11}$$

$$\mathbf{f}'(x,r,t) = \hat{\mathbf{f}}(x,r)e^{\lambda t}, \tag{12}$$

$$\hat{\mathbf{f}}(x,r) = -\alpha\left(\frac{\bar{\mathbf{u}}\cdot\hat{\mathbf{u}}}{||\bar{\mathbf{u}}||}\bar{\mathbf{u}} + ||\bar{\mathbf{u}}||\hat{\mathbf{u}}\right)\delta(x - x_c, r - r_c) \tag{13}$$

where α is a measure of the magnitude of the force.

Figures 6a and 6b show the magnitude of the steady and unsteady force as a function of the location of the control ring. The steady component is largest near the inlet because the baseflow velocities are high there, whereas the unsteady component is largest further downstream because the amplitude of the global mode is maximum there. We also notice that the unsteady component of the force is about an order of magnitude greater than the steady component. However, we know from equations (7) and (10) that the effect of the control ring on the unstable eigenvalue depends on the overlap of figures 5 and 6. We substitute the expressions in equations (11) and (13) into equations (7) and (10). The total change in the eigenvalue is given by the sum of the contributions from the steady and unsteady components

$$\delta\lambda_{total} = \delta\lambda_{\bar{\mathbf{F}}} + \delta\lambda_{\mathbf{f}'}. \tag{14}$$

In Figure 7, we plot the change in the eigenvalue as a function of the location of the control ring showing the total change as well as the contributions from the steady and unsteady components of the force on the same color scale. These figures identify the locations where passive control using the control ring would be most effective. There is a narrow region upstream of the bubble where the control ring will stabilise the flow and a much larger region downstream of the bubble where the control ring will destabilise the flow. These figures also show that the contribution from the steady component is significantly larger than the contribution from the unsteady component.

V. DYNAMICS OF THE CONTROLLED SYSTEM

We now verify whether the behaviour predicted by our linear sensitivity analysis actually occurs. We model the
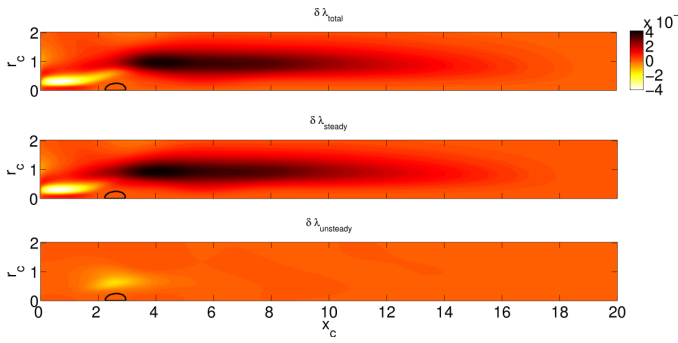
Fig. 7. The change in the eigenvalue as a function of the location of the control ring, from top (a) Total change, (b) Contribution from the steady component of the force and (c) Contribution from the unsteady component of the force. The figures have the same color scale. Light regions indicate regions of stabilisation, whereas dark regions indicate regions of destabilisation. The thick black line indicates the vortex breakdown bubble.

presence of a small control ring at $(x_c, r_c) = (0.66, 0.33)$. This corresponds to the centre of the region of stabilisation in Figure 7(a).

We choose a value of $\alpha = 0.1$ and add the forcing term in equation (11) to our nonlinear equations. We obtain a new steady baseflow and study the linear dynamics of the controlled system. Figure 8 compares the spectrum of the controlled system with that of the uncontrolled system. We notice that the unstable eigenvalue has been stabilised. Our linear sensitivity analysis predicts the eigenvalue of the system with a control ring at $(x_c, r_c) = (0.66, 0.33)$ to be $-0.021 + 2.120i$ which agrees well with the value obtained from the stability analysis of the controlled system, $-0.018 + 2.119i$.

The dynamics of the controlled and uncontrolled system can also be seen in Figure 9. We superpose small amplitude random-noise perturbations on the steady baseflows for the controlled and uncontrolled systems and monitor the energy of these perturbations over time. In the uncontrolled system, following some initial transient phase, these perturbations grow linearly. In the controlled system, these perturbations decay linearly.

VI. APPLICATIONS AND FURTHER WORK

In the previous section, we demonstrated that this approach to the control of spiral vortex breakdown works in theory. We now consider some of the practical issues related to this approach.

Practical engineering applications feature flows at much higher Reynolds numbers than that considered in this paper. In such cases, obtaining a steady baseflow would be very difficult and it might be easier and more relevant to carry out a sensitivity analysis around the mean flow. This would not be mathematically rigorous but could still provide valuable
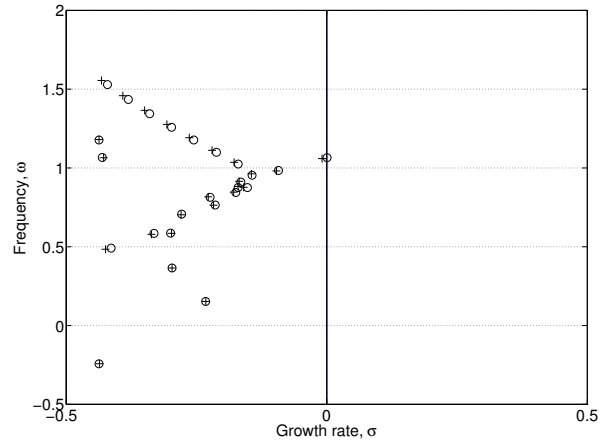

Fig. 8. Spectrum of the linear operator $\mathbf{L}$ for $m = -1$ for the uncontrolled (o) and controlled (+) baseflows, showing the 25 least stable eigenvalues. The marginally unstable eigenvalue in the uncontrolled flow is stable in the controlled flow.
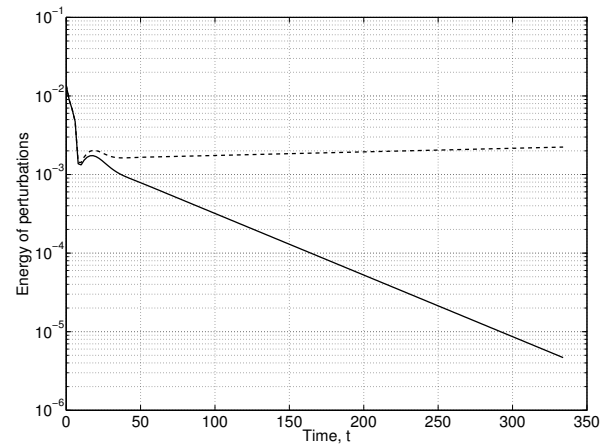

Fig. 9. The evolution of the energy of perturbations for $m = -1$ on top of the baseflows for the uncontrolled (dashed) and controlled (solid) system.

practical information for designers.

The control ring concept that we have used here is a simple model for a control device. An example of something similar that could be used in practice is a hot wire that forms an axisymmetric ring centred on the axis. The sensitivity of the location of the hot wire to the temperature and velocity can be obtained from the relevant adjoint fields, (namely, the adjoint temperature $\bar{T}^+$ and the adjoint momentum $\bar{\mathbf{m}}^+$. We have chosen to demonstrate this technique for vortex breakdown in an open domain. However, it can just as easily be applied to the control of vortex breakdown in a closed vessel (such as a combustion chamber). In this case, the adjoint pressure $\bar{p}^+$ can be used to obtain the sensitivity to mass injection. This would offer insight into how active control techniques such as blowing or suction could be used to control spiral vortex

breakdown.

The tools that have been developed here are now being applied to study swirling flows with variable density and combustion. The overall aim of this project is to develop the capability of producing sensitivity maps of real fuel injectors in combustion chambers. These sensitivity maps would give information about where the design should be changed to promote or suppress certain flow behaviours, taking into account the physical mechanisms that act in the flow.

VII. Conclusions

In this paper, we have considered a theoretical approach to the control of spiral vortex breakdown. We have shown that spiral vortex breakdown is caused by an unstable eigenmode that grows on top of the steady axisymmetric vortex breakdown bubble. We have used a Lagrangian approach to identify regions where the flow is most sensitive to small steady and unsteady (harmonic) forces. We have found that the regions upstream of the vortex breakdown bubble are most sensitive to steady and unsteady forces.

We then considered passive control using a small control ring placed in the flow. We have identified regions where this control device should be placed to stabilise or destabilise the flow. We have found that there is a narrow region upstream of the bubble where the control ring will stabilise the flow. We have verified this using numerical simulations.

The results from this study have shown that a linear sensitivity analysis can provide useful information for control, based on the underlying physics of the flow. This technique can be easily extended to control spiral vortex breakdown in more complicated geometries.

References

[1] D. H. Peckham and S. A. Atkinson, "Preliminary results of low speed wind tunnel tests on a gothic wing of aspect ratio 1.0," Aeronautical Research Council, Tech. Rep., 1957.

[2] M. Ruith, P. Chen, E. Meiburg, and T. Maxworthy, "Three-dimensional vortex breakdown in swirling jets and wakes: direct numerical simulation," *Journal of Fluid Mechanics*, vol. 486, pp. 331–378, JUL 10 2003.

[3] F. Gallaire, M. Ruith, E. Meiburg, J. Chomaz, and P. Huerre, "Spiral vortex breakdown as a global mode," *Journal of Fluid Mechanics*, vol. 549, pp. 71–80, FEB 25 2006.

[4] A. M. Mitchell and J. Délery, "Research into vortex breakdown control," *Progress in Aerospace Sciences*, vol. 37, no. 4, pp. 385–418, 2001.

[5] D. Hill, "A theoretical approach for analyzing the re-stabilization of wakes," *AIAA Paper 92-0067*, 1992.

[6] O. Marquet, D. Sipp, and L. Jacquin, "Sensitivity analysis and passive control of cylinder flow," *Journal of Fluid Mechanics*, vol. 615, pp. 221–252, NOV 25 2008.

[7] P. Meliga, D. Sipp, and J.-M. Chomaz, "Open-loop control of compressible afterbody flows using adjoint methods," *Physics of Fluids*, vol. 22, no. 5, MAY 2010.

[8] D. Sipp, O. Marquet, P. Meliga, and A. Barbagallo, "Dynamics and control of global instabilities in open flows: a linearized approach," *Applied Mechanics Reviews*, vol. 63, no. 030801, 2010.

[9] W. J. Grabowski and S. A. Berger, "Solutions of Navier-Stokes equations for vortex breakdown," *Journal of Fluid Mechanics*, vol. 75, no. JUN11, p. 525, 1976.

[10] O. Marquet, D. Sipp, L. Jacquin, and J.-M. Chomaz, "Multiple timescale and sensitivity analysis for the passive control of the cylinder flow," in *AIAA Paper 2008-4228*, 2008.